photonics

MDPI

Article

A Refined Methodological Approach for Terahertz Spectroscopy of Liquid Biosamples

Deborah Amos Adigun [1,*], Mikhail Gorbun [1], Aadya Menon [2], Janna Pennanen [1], Polina Kuzhir [1] and Georgy Fedorov [1]

[1] Department of Physics and Mathematics, Center for Photonics Sciences, University of Eastern Finland, Yliopistokatu 2, 80101 Joensuu, Finland; mikhail.gorbun@uef.fi (M.G.); janna.pennanen@uef.fi (J.P.); polina.kuzhir@uef.fi (P.K.); georgy.fedorov@uef.fi (G.F.)

[2] School of Computing, University of Eastern Finland, Länsikatu 15, 80110 Joensuu, Finland; aadya.menon@uef.fi

* Correspondence: adigun.deborah.amos@uef.fi

Abstract

Terahertz time-domain spectroscopy (THz-TDS) has emerged as a powerful tool for probing hydrated materials and biological tissues, where water dynamics dominate the dielectric response. This study focuses on improving the methodology of THz-TDS by replacing conventional cuvettes, which introduce unwanted absorption, reflections, and liquid bubbles that must be accounted for during measurement interpretation, with nitrocellulose membranes of various pore sizes. The membranes were hydrated with deionized water and sealed with food-grade cling film, and their transmission properties were measured using THz-TDS. To interpret the measurements, transfer matrix method simulations were performed using the optical constants of water reported by some experimentalists, allowing verification of our data. The findings for deionized water highlight the reliability of the methodology. Our results demonstrate that nitrocellulose membranes provide stable and reproducible transmission measurements in good agreement with theoretical reference models, supported by weight retention studies and reproducibility tests conducted in spatial, temporal, and random measurement conditions. These improvements contribute to the development of more robust THz-TDS approaches for hydrated biological materials and suggest future applications in non-invasive tissue hydration monitoring and biomedical diagnostics.

Keywords: Terahertz spectroscopy; THz-TDS; dielectric function; nitrocellulose membrane; transfer matrix method; deionized water; biological tissues

Check for updates

Received: 22 February 2026
Revised: 26 March 2026
Accepted: 7 April 2026
Published: 14 April 2026

Copyright: © 2026 by the authors. Licensee MDPI, Basel, Switzerland. This article is an open access article distributed under the terms and conditions of the Creative Commons Attribution (CC BY) license.

1. Introduction

Terahertz (THz) technology has gained growing attention as a powerful tool bridging the gap between electronics and photonics [1]. Operating in the 0.1–10 THz frequency range, THz radiation is non-ionizing, highly sensitive to polar molecules, and capable of probing low-energy excitations in matter [2]. These characteristics have led to applications in material science, security screening, and, increasingly, biomedical diagnostics [3,4]. The development of reliable terahertz methodologies for liquid biosamples is an ongoing area of research, as most biological samples, including saliva, blood plasma, urine and tears, are water-based. Accordingly, the focus of this study is not the investigation of water itself, but the establishment of a refined experimental approach for liquid biosample THz

measurements. Water is used as a reference model due to its dielectric response in the THz range from previous studies, enabling direct comparison with our experimental results.

From a practical point of view, this frequency range is often called the THz gap, which lies between the microwave and infrared regions. Until recently, the gap was technologically underutilized as a result of a lack of efficient sources and detectors. However, advances in photoconductive antennas, femtosecond laser systems, and nonlinear optical materials have enabled broadband terahertz time-domain spectroscopy (THz-TDS) systems capable of probing this range with high signal-to-noise ratios [5]. The 0.2–2 THz range is also favorable for non-destructive evaluation, security screening, and material characterization due to its moderate penetration through dielectrics, polymers, and biological tissues, while remaining non-ionizing [6]. In addition, many materials exhibit distinct spectral "*fingerprints*" in this range, allowing for spectral discrimination and chemical identification. This is especially important in pharmaceuticals, biomedical diagnostics, and explosives detection [7].

Most studies employ window-based liquid cells to control sample thickness [8], while others highlight membrane-based approaches to reduce multiple reflections and background interference [9]. A frequently used substrate in optical and THz spectroscopy is crystalline quartz, i.e., cuvettes, primarily due to its mechanical and optical stability. However, quartz is suboptimal for THz applications that exhibit a relatively high refractive index in the THz range ($n \approx 1.9$–2.1) [10], causing substantial reflection losses at the interface with air. These limitations are particularly problematic when studying water and hydrated bio-tissues, where background substrate effects can overshadow delicate dielectric features. Chua et al. [11] were among the first to employ THz-TDS in transmission mode to measure the absorption spectra of wheat particles within the 0.1–2.0 THz frequency range. They analyzed the difference between the spectra of wet and dried wheat samples to explore how absorption correlates with the moisture content. Zahid et al. [12] utilized THz absorption spectra to monitor the water content and properties in plant leaves over a four-day period. By calculating dielectric constants, they observed an increase in the transmissivity of THz waves in leaf samples over time, alongside reductions in leaf weight and thickness, as well as morphological changes in both fresh and water-stressed leaves. Markelz [13] provided a comprehensive review of the application of THz spectroscopy to investigate biomolecular structure and function. The paper highlighted how dielectric responses depend on collective vibrational modes and relaxation processes, emphasizing the influence of temperature, hydration, molecular binding, and conformational changes.

In the THz frequency range (0.1–10 THz), water exhibits visible absorption properties due to its rotational and vibrational degrees of freedom. These include librational motions (restricted rotations), relaxation processes of the molecular dipole, and collective hydrogen-bond network vibrations [14]. This makes water both a challenge and an opportunity in THz spectroscopy transmission due to high absorption, but it also serves as a sensitive probe for studying hydration dynamics and interactions in biological systems [13,15].

Understanding water's interaction with THz radiation is crucial for applications ranging from biomolecular hydration-shell analysis to non-invasive detection of water content in pharmaceutical and agricultural materials [16]. Moreover, characterization of the complex dielectric function of water has become a basis of THz spectroscopy because water dominates absorption in the THz and microwave regions. One of the foundational contributions came from Buchner et al. [17], who provided empirical measurements of the dielectric properties of water across a broad frequency spectrum, from megahertz (MHz) to gigahertz (GHz). Their study focused on dielectric relaxation behavior in bulk water at room temperature and low frequency ranges, using vector network analyzer techniques. This data served as a basis for understanding water's dipolar relaxation and laid the groundwork for extrapolation to higher frequencies.

In the context of this work, the use of deionized water (DIW) on nitrocellulose (NC) membranes/substrates serves as a simplified model system for characterizing the dielectric properties of hydrated biological tissues. Leveraging previously obtained data on dielectric properties of water [18,19] for simulation and fitting provides a strong theoretical foundation for extracting and interpreting dielectric functions from experimental THz-TDS data. The complex dielectric function was evaluated using

$$\varepsilon(w) = \eta^2, \tag{1}$$

where

$$\eta = n + i\kappa. \tag{2}$$

Here, $\varepsilon(\omega)$ is the complex frequency-dependent dielectric function, η is the complex refractive index, n is the real part of the refractive index describing wave propagation in the medium, κ is the extinction coefficient accounting for absorption losses, and i is the imaginary unit.

NC membranes have emerged as a viable alternative sample-holding substrate in THz-TDS, especially when working with minute quantities of biological material or aqueous solutions. Zhao et al. [9] demonstrated the effectiveness of NC membranes for detecting α-lactose in aqueous media using THz-TDS, noting their compatibility with small sample volumes and reduced signal attenuation compared to conventional polyethylene pellets or liquid cells. Their study explored membranes of varying pore sizes (0.1 μm, 0.2 μm, and 0.45 μm), finding that increased pore size generally led to stronger absorption peaks. The hydrophilic nature and biological compatibility of NC membranes, together with their low THz background response, make them highly suitable for bio-spectroscopic applications. This is particularly advantageous for the direct measurement of hydrated specimens, where conventional liquid handling cells often introduce additional complexity.

This work addresses challenges related to measuring transmission spectra of liquid samples in the THz range. Using THz-TDS, we investigate transmission spectra of water confined within a porous NC membrane. Specifically, for confining liquid samples in THz-TDS, we investigate the use of porous NC membranes as an alternative to cuvettes. Compared with crystalline quartz, NC membranes provide low background absorption, strong water retention, and reduced Fresnel reflection losses, rendering them promising substrates for hydrated bio-spectroscopy [9]. Using experimental THz-TDS measurements of DIW confined within NC membranes, we benchmark measured transmission response against established optical and dielectric reference data reported by Bertie and Lan [18] and Zhou et al. [19]. To compare simulated and experimental transmission spectra, we modeled the dielectric responses via the transfer matrix method (TMM).

In this work, we focus on methodological innovations in spectroscopy with THz transmission, especially in terms of substrate material choice, sample containment, and signal processing with analysis in the 0.2–2 THz range. This frequency window has emerged as a core operational range in THz spectroscopy and imaging. The reason is its unique balance between penetration depth, spectral resolution, and source/detector availability. This spectral region corresponds to photon energies of approximately 0.8 to 4 meV, which align well with low-frequency molecular vibrations, phonon modes, hydrogen bonding dynamics, and rotational modes of polar molecules [16]. As such, it is susceptible to collective dynamics in biomolecules, liquid water, hydrogen-bonded networks, and low-energy excitations in semiconductors and dielectrics [20].

Unlike conventional liquid cells that rely on rigid cuvettes with fixed path lengths, the present work introduces a membrane-confined, sealed liquid configuration that minimizes multiple reflections and bubble formation. The novelty of this study lies in experimentally

validating this configuration through systematic pore size comparison, gravimetrically determined effective thickness, and transfer matrix analysis to assess spectral consistency. The goal is not to redefine water dielectric properties, but to establish a robust methodology for hydrated biological samples in THz-TDS measurements.

2. Materials and Methods

THz-TDS was employed as the primary spectroscopic technique to investigate hydrated NC membranes. Unlike intensity-based spectroscopies, THz-TDS measures the transient electric field of a THz pulse in the time domain, enabling extraction of both amplitude and phase information [21]. Broadband THz pulses (0.2–3 THz) were generated and detected using photoconductive antennas gated by sub-100 fs near-infrared (NIR) pulses. This configuration provided sub-picosecond resolution, essential for determining the complex transmission spectra of aqueous samples.

2.1. Experimental Setup

A schematic of the setup is shown in Figure 1, and the corresponding operational principle is presented in Section 2.2. The femtosecond laser pulse is split into pump and probe arms by a beam splitter. The pump beam excites the transmitter antenna (TA), generating a THz pulse, which propagates through the sample and is detected at the receiver antenna (RA). The probe beam is directed through a delay stage to introduce a variable optical path length, enabling temporal sampling of the THz waveform. To reduce moisture, the entire system is enclosed in a purge box flushed with dry air.

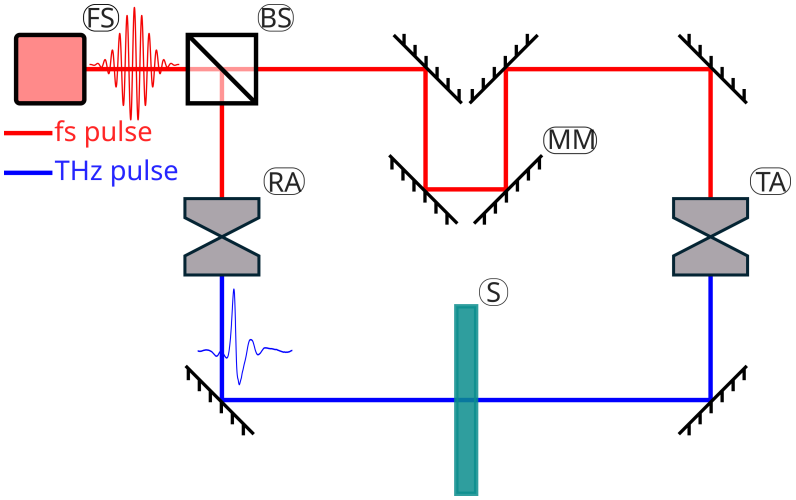
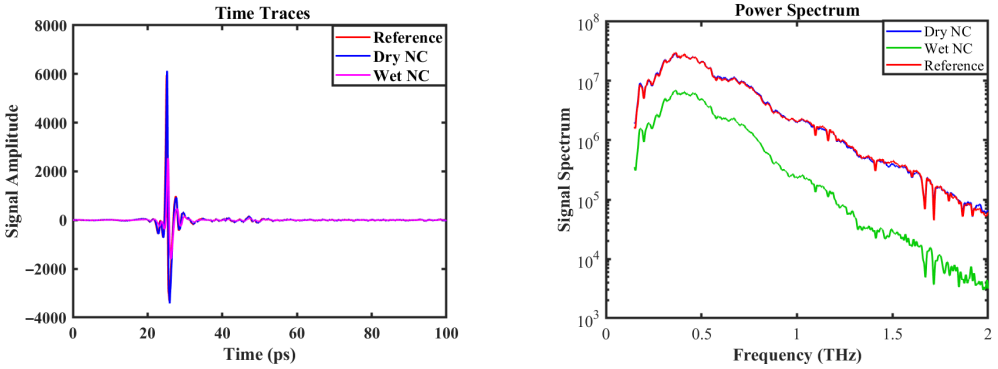


Figure 1. Schematic of the THz-TDS setup. A femtosecond laser pulse (red) is split into a pump and a probe. The pump excites the transmitter antenna (TA), generating a THz pulse (blue), which passes through the sample (S) before reaching the receiver antenna (RA). The probe pulse passes through a delay stage with a movable mirror (MM) to temporally sample the THz pulse at the detector.

The THz-TDS system was driven by a femtosecond laser source operating at 780 nm with a pulse duration of 80 fs, repetition rate of 80 MHz, and average output power of 140 mW. THz radiation was generated and detected using photoconductive antennas based on GaAs on Si-GaAs, biased at a $\pm$40 V square wave signal.

The measured time-domain THz pulse and its corresponding Fourier amplitude spectrum are shown in Figure 2. The usable spectral bandwidth extends from approximately 2 to 4 THz, with a central frequency near 0.4 THz. These parameters define the effective frequency window for the transmission measurements reported in this study.



(**a**) Time-domain THz pulse. (**b**) Fourier spectrum (power spectrum).

Figure 2. Measured signals during THz measurements.

2.2. Operational Principle

At the transmitter, the pump beam illuminated a biased photoconductive antenna, producing a broadband THz pulse. This pulse traversed the sample before reaching the receiver antenna. The probe beam, time-delayed using a movable mirror in the delay stage, reached the receiver antenna and generated photo-excited carriers. The measured photocurrent was proportional to the instantaneous electric field of the THz pulse. Scanning the delay enabled reconstruction of the complete time-domain waveform.

2.3. Sample Preparation

Porous NC membranes (Amersham Protran, Cytiva, Marlborough, MA, USA) with pore sizes of 0.1, 0.2, and 0.45 µm were used as sample substrates [22]. Membranes were hydrated by immersion in deionized water (DIW) until saturated and then sealed between polyethylene films (food-grade cling film) to reduce evaporation during measurement. Figure 3 shows a scheme of the NC membrane with and without the sample.

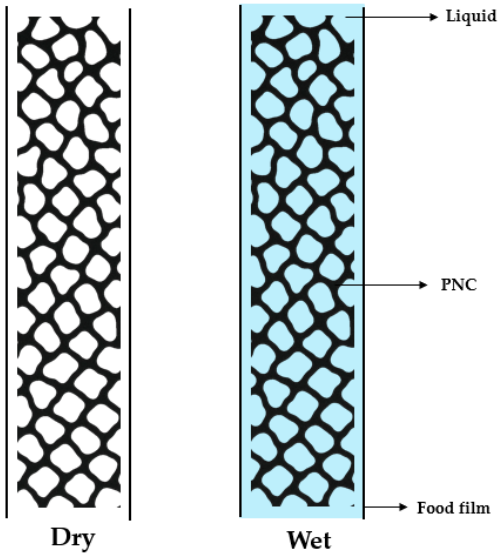
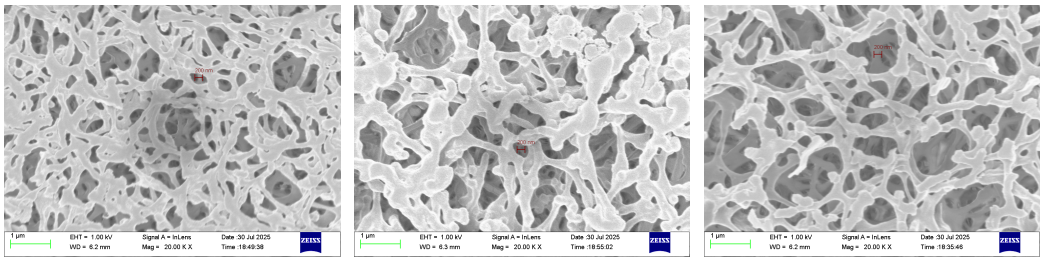


Figure 3. Schema showing NC membrane with and without the liquid sample.

Scanning Electron Microscopy (Zeiss LEO Gemini 1550, Carl Zeiss AG, Oberkochen, Germany) was used to visualize the surface morphology and pore structure of the NC membranes (Figure 4). A thin conductive coating of chromium was deposited onto the membrane surface via sputtering. This step was necessary to prevent surface charging under the electron beam, which can otherwise distort the imaging of non-conductive

polymeric samples. The sputter-coated membranes were then imaged under high vacuum, allowing a clear resolution of the pore distribution and membrane texture.



(**a**) 0.1 µm pore size (**b**) 0.2 µm pore size (**c**) 0.45 µm pore size

Figure 4. Visualization of different porous NC membrane pore sizes using SEM.

Rationale for Selection

NC membranes were chosen over quartz substrates due to:

1. Low Reflectance: Their refractive index is closer to water and air, reducing Fabry-Pérot interference [23].
2. Biological Relevance: Widely used in biochemical assays, NC membranes provide physiologically relevant hydration environments [9,24,25].
3. Hydration Retention: The porous matrix of NC membranes preserves water during measurement, simulating the hydration states of biological tissues.

2.4. Sample Holder

The samples were mounted on a custom steel aperture plate (Figure 5) with nine circular apertures (3 mm diameter, 10 mm spacing). The aperture diameter exceeded the THz wavelength, satisfying Rayleigh criteria for transmission measurements.

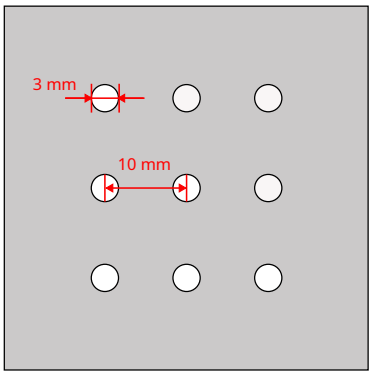


Figure 5. Aperture plate used for sample mounting. Nine apertures (3 mm diameter) enabling simultaneous placement of samples and leaving an aperture open for reference measurements.

2.5. Water Effective Thickness Measurements

To model wave propagation through a water layer, the thickness of the water is a required parameter. We took measurements of water weight absorbed by different pore sizes with different areas using the Sartorius 2432 balance (Sartorius AG, Göttingen, Germany). The effective height of the water (DIW) was calculated using Equation (3), which was equated to the thickness of the water.

$$H_{eff} = \frac{\text{Mass of Water}}{\text{Area of Paper} \times \text{Density of Water}}. \quad (3)$$

The resulting data are presented in Table 1 and Figure 6 below.

Table 1. DIW weight measurement of diffferent pore sizes.

Pore Size (μm)	Area (cm^2)	Dry Paper (g)	Wet Paper (g)	Water (g)	Height (μm)
0.1	1	0.3285	0.3355	0.0070	70
	2	0.3328	0.3482	0.0154	77
	3	0.3383	0.3614	0.0231	77
	4	0.3446	0.3744	0.0298	75
	6	0.3551	0.4022	0.0472	79
	7.5	0.3639	0.4201	0.0562	75
	9	0.3727	0.4398	0.0671	75
0.2	1	0.3281	0.3367	0.0086	86
	2	0.3332	0.3498	0.0165	83
	3	0.3384	0.3629	0.0244	81
	4	0.3446	0.3776	0.0331	83
	6	0.3547	0.4051	0.0504	84
	7.5	0.3621	0.4254	0.0633	84
	9	0.3703	0.4483	0.0779	87
0.45	1	0.3263	0.3339	0.0076	76
	2	0.3303	0.3456	0.0154	77
	3	0.3340	0.3575	0.0235	78
	4	0.3382	0.3684	0.0302	75
	6	0.3468	0.3917	0.0449	75
	7.5	0.3534	0.4102	0.0568	76
	9	0.3596	0.4271	0.0675	75

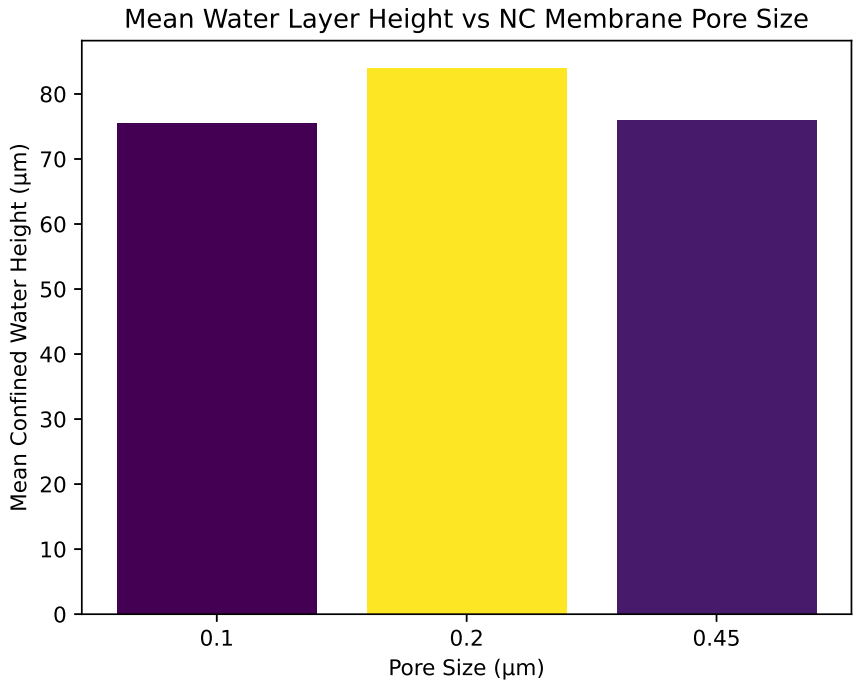


Figure 6. Water effective thickness.

2.6. Measurements and Data Acquisition

The laser system was stabilized by a warm-up period of 90 min before data collection. The samples were aligned on the aperture plate, leaving one aperture uncovered (empty) for reference measurements. To minimize terahertz radiation absorption by water vapor, the purge box was flushed with dry air for 90 min prior to measurements.

The recorded THz signals (as shown in Figure 2) were acquired in the time domain as the electric field $E(t)$ transmitted through the sample and through an empty reference aperture. Each time-domain waveform (time trace) was converted to the frequency domain by applying a discrete Fourier transform,

$$S(\omega_k) = \Delta t \sum_{n=0}^{N-1} E(t_n)\, e^{-i\omega_k t_n}, \tag{4}$$

where $t_n = n\Delta t$ is the discrete time sampling, Δt is the temporal step size, N is the total number of samples, and $\omega_k = \frac{2\pi k}{N\Delta t}$ is the discrete angular-frequency grid. Applying this transform to the sample and reference signals yields the spectra $S_s(\omega)$ and $S_r(\omega)$, respectively. The frequency-dependent transmission spectrum was then obtained as

$$T(\omega) = \frac{|S_s(\omega)|^2}{|S_r(\omega)|^2}. \tag{5}$$

2.7. Simulation Using Optical Constants from Other Works

Bertie and Lan [18] presented one of the most detailed experimental characterizations of the optical constants of liquid water in the far-infrared-to-THz region. Their study provided tabulated data for the real (n) and imaginary (κ) components of the complex refractive index, derived from highly controlled absorbance and reflectance measurements of water layers using Attenuated Total Reflection (ATR) and Fourier transform infrared (FTIR) spectroscopy. Also, Zhou et al. [19] conducted a systematic study of THz-TDS transmission of liquid water to quantify how its optical and dielectric properties vary with temperature. Using a temperature-controlled THz time-domain system (0.2–2.4 THz), they measured the refractive index, absorption coefficient, and complex dielectric function of water across 275–340 K. Their results showed clear increases in refractive index, absorption, and dielectric constant with rising temperature, reflecting changes in hydrogen bond dynamics and molecular relaxation processes. The experimental data were well reproduced by a double-Debye relaxation model, confirming its suitability to describe the water temperature-dependent THz response.

These optical constants are directly relevant for simulating THz transmission spectra through water. In this work, the data provided by Bertie et al. and Zhou et al. at room temperature were imported into MATLAB R2023b and used on the dielectric function given in Equations (1) and (2) to simulate transmission, which served as the *theoretical model* against which our experimental THz spectra were fitted.

2.7.1. Transfer Matrix Method (TMM)

To model wave propagation through a water layer of thickness $d \approx 75$ and 85 μm, the TMM is applied. This approach accounts for multiple reflections and interference effects at interfaces between layers of different refractive indices [26]. In our case, the multilayer system consists of:

- Incident Medium: Air ($n = 1$);
- Sample Layer: Liquid water (complex $n = n_{real} + i \cdot n_{imag}$);
- Exit Medium: Air.

The magnitude of the wave vector (wavenumber) in vacuum is defined as

$$k = \frac{\omega}{c}. \tag{6}$$

Each interface introduces Fresnel reflection and transmission, and each layer adds a propagation phase delay. The model computes the net forward and backward amplitudes using the continuity of fields across boundaries (Figure 7).

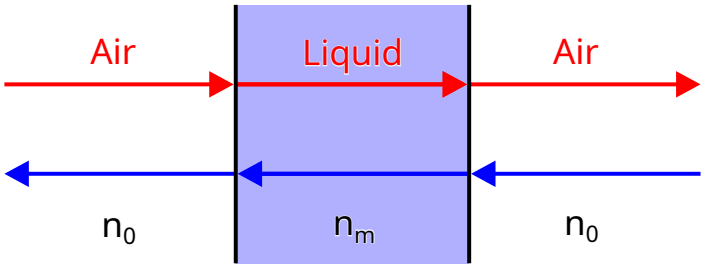


Figure 7. Schematics of multilayer system.

The Fresnel equations are based on boundary conditions of **D**, **H**, **E** and **B** (Maxwell's equations), assuming $\vec{k}$ is perpendicular to the direction of the propagating field. The electromagnetic wave is represented by two complex amplitudes: a forward-traveling wave (a) and a backward-traveling wave (b). The subscripts on these amplitudes (e.g., a_{L} and b_{R}: L—left; R—right) denote their position relative to a boundary.

For the border: At an interface between two media with refractive indices $n_0 = 1$ and n_{m}, the amplitudes are related by the continuity of the tangential electric and magnetic fields. For a wave traveling from the left to the right, the amplitudes are on the left ($a_{\mathrm{L}}, b_{\mathrm{L}}$) and right ($a_{\mathrm{R}}, b_{\mathrm{R}}$) of the boundary. So, for the border, as illustrated in Figure 8, we apply

$$a_{\mathrm{L}} = \frac{1}{2}\left(a_{\mathrm{R}}\left(1 + \frac{n_{\mathrm{m}}}{n_0}\right) + b_{\mathrm{R}}\left(1 - \frac{n_{\mathrm{m}}}{n_0}\right)\right), \tag{7}$$

$$b_{\mathrm{L}} = \frac{1}{2}\left(a_{\mathrm{R}}\left(1 - \frac{n_{\mathrm{m}}}{n_0}\right) + b_{\mathrm{R}}\left(1 + \frac{n_{\mathrm{m}}}{n_0}\right)\right). \tag{8}$$

For propagation through a layer of thickness d and complex refractive index η, a propagation factor is introduced to account for phase accumulation and magnitude reduction between boundaries (Figure 9):

$$a_{\mathrm{new}} = a_{\mathrm{old}} \cdot \exp(-ik\eta_m d), \tag{9}$$

$$b_{\mathrm{new}} = b_{\mathrm{old}} \cdot \exp(ik\eta_m d). \tag{10}$$

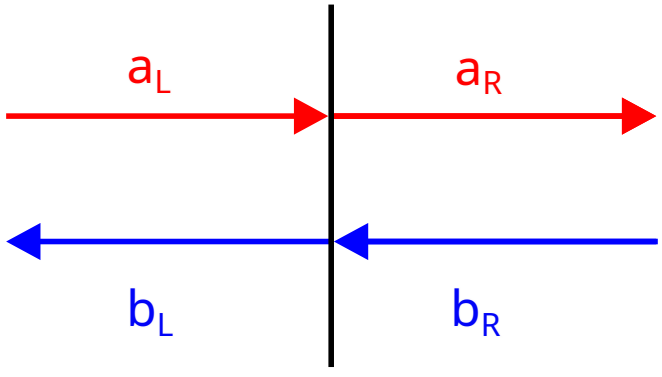


Figure 8. Schema of transmission at border.

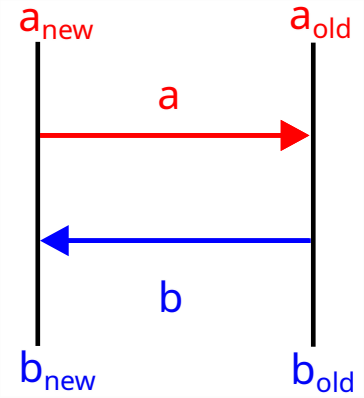


Figure 9. Schema for phase accumulation.

2.7.2. Simulation Procedure and Resulting Spectra

The simulation is performed by sequentially applying the transfer matrix method across each interface and layer. We impose the boundary conditions such that the transmitted wave amplitude in the exit medium is normalized to unity ($a_{\text{transmitted}} = 1$) and assume that there is no backward-propagating wave in the exit region ($b_{\text{exit}} = 0$). Under these conditions, the corresponding incident a_{incident}) and reflected ($b_{\text{reflected}}$) amplitudes at the input interface are calculated.

The transmission coefficient is finally computed from the corresponding amplitude:

$$T(f) = \left| \frac{1}{a_{\text{incident}}} \right|^2. \tag{11}$$

The reflection coefficient is determined by the amplitude of the reflected wave ($b_{\text{reflected}}$) relative to the incident wave:

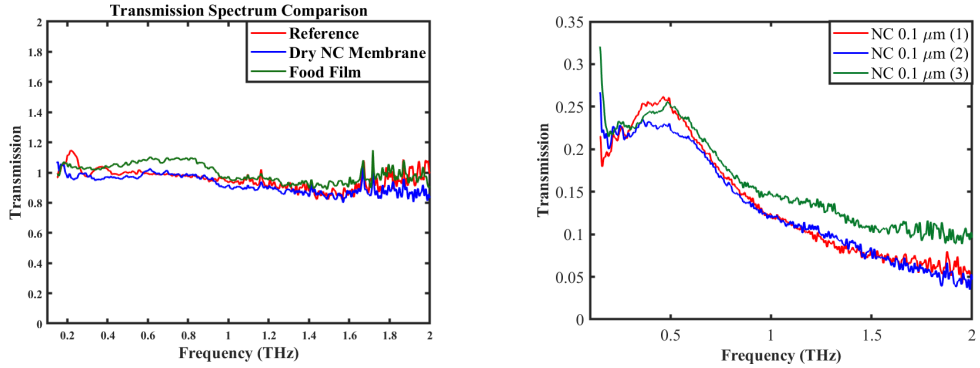
$$R(f) = \left| \frac{b_{\text{reflected}}}{a_{\text{incident}}} \right|^2. \tag{12}$$

This procedure provides a detailed spectral response of the water layer, allowing for the characterization of its optical behavior across the frequency range of interest using our experimental data.

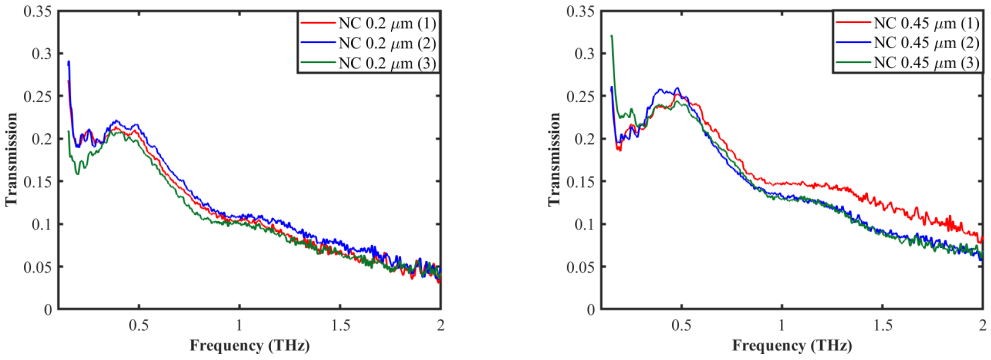
3. Results

In THz-TDS, the selection of sample substrates and sealing materials must be chosen carefully because any component placed in the THz path can introduce absorption, scattering, or reflection that distorts the measurement of interest. To ensure accurate interpretation of spectral features, especially in hydrated or biological samples, it was essential to first evaluate the intrinsic transparency of supporting and sealing materials. We plotted the transmission spectra of the empty open aperture (reference), dry NC membrane, and food-grade cling film together. This was done to confirm that they are transparent and will not interfere with our liquid sample measurements.

From Figure 10a, we see that the transmission is close to 1 with a 10% error. This is not perfectly 1 and can even exceed 1 because of the irreproducibility of our setup. However, this confirms that the food-grade cling film, dry NC membrane, and empty (open) aperture will not interfere with our liquid sample measurements.



(**a**) THz Transparency Assessment (**b**) 0.1 µm pore sized membrane



(**c**) 0.2 µm pore sized membrane (**d**) 0.45 µm pore sized membrane

Figure 10. (**a**) Transmission spectra of NC membranes (dry) and food-grade cling film relative to an empty aperture. (**b**–**d**) Mean transmission spectra of DIW confined in NC membranes of different pore sizes.

Experimental Results

The measurements were carried out on three samples each of the different pore sizes. We immediately sealed these samples with the food-grade cling film to avoid evaporation during measurements. Afterwards, we calculated the mean of five measurements of each sample with different pore sizes. The results are presented in Figure 10.

To evaluate potential thickness variations caused by membrane swelling or nonuniform sealing, transmission measurements were performed in different regions of the same hydrated membrane. The resulting spectra, shown in Figure 10b–d, are identical, indicating that any local variations in effective thickness have a negligible impact on the measured THz transmission.

The extraction of the complex refractive index and absorption coefficient from transmission measurements requires solving inverse problems involving transcendental equations. In practice, this procedure is highly sensitive to small uncertainties in experimental parameters, including sample thickness, phase noise, and amplitude fluctuations. In the present case, the combination of strong water absorption in the THz range and the thin, membrane-confined geometry further amplifies these sensitivities, leading to significant instability in the extracted optical constants.

For this reason, rather than performing a direct inversion that may introduce nonphysical artifacts, we adopt a forward-modeling approach. Specifically, we compute transmission spectra using transfer matrix simulations based on independently reported dielectric functions (Bertie and Lan [18]; Zhou et al. [19]) and directly compare these with our experimental measurements.

The experimental transmission spectra are found to lie within the range predicted by these literature datasets and exhibit consistent frequency-dependent behavior. This agreement provides a validation of the proposed methodology while avoiding the uncertainties associated with inverse extraction procedures.

4. Discussion

To contextualize and validate the experimental transmission measurements, previously reported optical constants of liquid water were used as reference data. Specifically, optical constants reported by Bertie and Lan [18] and measurements of dielectric properties at room temperature reported by Zhuo et al. [19] were used. These datasets were used to calculate reference transmission spectra using the transfer matrix method, enabling direct comparison with the experimentally measured spectra. It is important to note that dielectric functions of water reported in the THz range of Bertie and Zhou's experiment exhibit noticeable differences. When these datasets are used in transfer matrix simulations, they generate distinct transmission curves, as shown in Figure 11. The experimentally measured transmission in our work lies within this reported range and follows the same frequency-dependent trend. This consistency supports the physical reliability of the proposed membrane-based methodology.

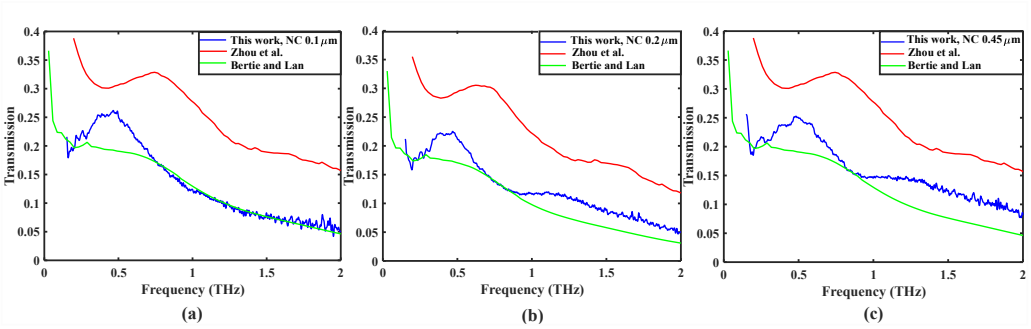


Figure 11. Transmission spectrum: Experimental results vs. theoretical reference [18,19]. (**a**) NC 0.1 μm pore size, (**b**) NC 0.2 μm pore size, (**c**) NC 0.45 μm pore size.

The non-monotonous frequency dependence can be explained as a manifestation of Debye relaxation in water, as explained in the paper [27]. Discussion of these phenomena is out of scope of the current work devoted to the methodology of THz spectroscopy of liquid samples.

The transmission measurements demonstrate a high degree of reproducibility for water confined within porous NC membranes. As shown in Figure 10, three independently prepared samples for each membrane thickness exhibit nearly identical transmission spectra, indicating that the sample preparation procedure and measurement protocol are reliable and stable. This reproducibility is a key requirement for methodological development in THz spectroscopy of liquids.

At the same time, systematic differences are observed between membranes with different pore sizes. In particular, the overall transmission through water-filled membranes with pore sizes of 0.1 μm and 0.45 μm is higher than that observed for the 0.2 μm membrane. Although higher transmission may appear advantageous at first glance, this effect must be interpreted in the context of sample retention and effective liquid thickness within the porous matrix.

Based on experimental observations and sample handling behavior, the 0.2 μm NC membrane retains a larger and more stable amount of liquid water compared to the other pore sizes. This conclusion is supported by the mass measurements summarized in Table 1 and Figure 6, which show that the effective water content confined within the 0.2 μm membrane is higher. In contrast, membranes with larger pores (0.45 μm) exhibited increased

liquid leakage and evaporation during preparation and measurement, while the smallest pores (0.1 μm) likely limited uniform water distribution due to reduced permeability.

The intermediate pore size of 0.2 μm therefore provides a balance between permeability and liquid retention, promoting a more homogeneous distribution of water within the membrane structure. This results in a transmission response that is consistent and physically meaningful compared to the transmission spectra calculated using established dielectric properties of water, as illustrated in Figure 11. Importantly, the experimentally measured transmission spectra fall within the range defined by calculations based on previously reported optical constants, confirming that the membrane-confined water behaves as expected without introducing strong substrate-induced artifacts.

These findings support the use of porous NC membranes as an effective alternative to conventional liquid cuvettes for THz spectroscopy of liquid biosamples. The results further indicate that membrane pore size is a critical parameter influencing both sample stability and electromagnetic response. The present comparison provides a starting point for systematic investigations into how membrane morphology governs THz transmission, with direct implications for extending this methodology to more complex biological liquids.

To end, the usability of the NC membrane configuration was evaluated based on three criteria:

i. Consistency of the measured transmission spectra with the expected frequency-dependent absorption behavior of water;
ii. Reproducibility of measurements across different positions of the same hydrated membrane;
iii. Agreement with transfer matrix simulations based on previously reported dielectric datasets of water.

Together, these observations demonstrate that NC membranes provide a stable platform for THz-TDS measurements of confined liquid samples.

5. Conclusions

Because the pore sizes (0.1–0.45 μm) are much smaller than the THz wavelength (300 μm), the electromagnetic field does not resolve the internal microstructure of the membrane. The NC scaffold therefore does not introduce additional scattering or resonant contributions and acts primarily as a low-index, low-loss mechanical support. Under these conditions, the effective dielectric response of the hydrated membrane is governed predominantly by the liquid filling fraction, while the intrinsic dielectric contribution of the NC matrix introduces only a minor correction within experimental uncertainty. Representing the membrane as an effective liquid layer with reduced thickness thus directly reflects the actual liquid content rather than serving as an arbitrary fitting parameter. Therefore, explicitly introducing a full Effective Medium Theory formalism would not meaningfully alter the extracted liquid optical constants, since the THz response is dictated by the liquid properties and the NC scaffold is effectively transparent in this spectral range.

Beyond improved liquid handling, porous NC membranes exhibit favorable performance as THz sample-support substrates, providing a practical alternative to quartz cuvettes for liquid-based measurements. Due to their low refractive index and inherently porous structure, NC membranes substantially reduce Fresnel reflection losses compared to cuvettes. These properties are important to consider in the terahertz range where the free-space wavelength (≈300 μm at 1 THz) renders quartz interfaces highly reflective. The membranes enable stable confinement of micrometer-scale liquid layers while preserving the transmitted field amplitude required for reliable extraction of optical constants. Despite these advantages, the approach is limited by membrane pore morphology: viscous liquids or samples containing particles >100 nm cannot be reliably confined, and, for example,

blood cells are incompatible due to cellular dimensions exceeding the pore size. Within these constraints, porous NC membranes provide a technically robust, low-loss platform for THz spectroscopic probing of aqueous and plasma-based biosamples.

Author Contributions: Conceptualization, P.K. and G.F.; methodology, D.A.A., A.M. and J.P.; software, D.A.A., M.G. and A.M.; validation, D.A.A., M.G., A.M. and G.F.; formal analysis, D.A.A.; investigation, D.A.A., A.M. and G.F.; data curation, D.A.A.; writing—original draft preparation, D.A.A.; writing—review and editing, P.K.; visualization, D.A.A., M.G. and G.F.; supervision, G.F. and P.K.; project administration, G.F. and P.K.; funding acquisition, G.F. and P.K. All authors have read and agreed to the published version of the manuscript.

Funding: The work was supported by the Research Council of Finland (Flagship Programme PREIN, decision 368653; research project, decision 357033) and EU Horizon 2024 MSCA project 101236439 (HERMES).

Institutional Review Board Statement: Not applicable.

Informed Consent Statement: Not applicable.

Data Availability Statement: Data underlying the results presented in this paper are not publicly available at this time but may be obtained from the authors upon reasonable request.

Conflicts of Interest: The authors declare no conflicts of interest.

References

1. Nagatsuma, T. Terahertz technologies: Present and future. *IEICE Electron. Express* **2011**, *8*, 1127–1142. [CrossRef]
2. Chen, M.; Wang, Y.; Wang, X.; Li, L. Advances in terahertz detection and imaging. *Front. Phys.* **2022**, *10*, 855623. [CrossRef]
3. Wu, J.Z.; Li, X.Q.; Sun, L.J.; Liu, C.L.; Sun, X.R.; Yu, L. Advances in the application of terahertz time-domain spectroscopy and imaging technology in crop quality detection. *Spectrosc. Spectr. Anal.* **2022**, *42*, 358–367.
4. Zhang, L.; Zhang, M.; Mujumdar, A.S. Terahertz spectroscopy: A powerful technique for food drying research. *Food Rev. Int.* **2023**, *39*, 1733–1750. [CrossRef]
5. Zhang, X.-C.; Xu, J. *Introduction to THz Wave Photonics*; Springer: New York, NY, USA, 2010.
6. Ferguson, B.; Zhang, X.-C. Materials for terahertz science and technology. *Nat. Mater.* **2002**, *1*, 26–33. [CrossRef] [PubMed]
7. Siegel, P.H. Terahertz technology in biology and medicine. *IEEE Trans. Microw. Theory Tech.* **2004**, *52*, 2438–2447. [CrossRef]
8. Thrane, L.; Jacobsen, R.H.; Jepsen, P.U.; Keiding, S.R. THz reflection spectroscopy of liquid water. *Chem. Phys. Lett.* **1995**, *240*, 330–333. [CrossRef]
9. Zhao, X.; Liu, S.; Wang, C.; Zuo, J.; Zhang, C. Nitrocellulose membrane sample holder using for terahertz time domain spectroscopy. In *Infrared, Millimeter-Wave, and Terahertz Technologies IV*; SPIE: Bellingham, WA, USA, 2016; Volume 10030, pp. 404–409.
10. Naftaly, M.; Gregory, A. Terahertz and microwave optical properties of single-crystal quartz and vitreous silica and the behavior of the boson peak. *Appl. Sci.* **2021**, *11*, 6733. [CrossRef]
11. Chua, H.S.; Obradovic, J.; Haigh, A.D.; Upadhya, P.C.; Hirsch, O.; Crawley, D.; Gibson, A.A.P.; Gladden, L.F.; Linfield, E.H. Terahertz time-domain spectroscopy of crushed wheat grain. In Proceedings of the IEEE MTT-S International Microwave Symposium Digest, Long Beach, CA, USA, 12–14 June 2005; pp. 2103–2106.
12. Zahid, A.; Abbas, H.T.; Imran, M.A.; Qaraqe, K.A.; Alomainy, A.; Cumming, D.R.S.; Abbasi, Q.H. Characterization and water content estimation method of living plant leaves using terahertz waves. *Appl. Sci.* **2019**, *9*, 2781. [CrossRef]
13. Markelz, A.G. Terahertz dielectric sensitivity to biomolecular structure and function. *IEEE J. Sel. Top. Quantum Electron.* **2008**, *14*, 180–190. [CrossRef]
14. Heyden, M.; Sun, J.; Funkner, S.; Mathias, G.; Forbert, H.; Havenith, M.; Marx, D. Dissecting the THz spectrum of liquid water from first principles via correlations in time and space. *Proc. Natl. Acad. Sci. USA* **2010**, *107*, 12068–12073. [CrossRef]
15. Hobza, P.; Müller-Dethlefs, K. *Non-Covalent Interactions: Theory and Experiment*; No. 2; Royal Society of Chemistry: Cambridge, UK, 2010.
16. Jepsen, P.U.; Cooke, D.G.; Koch, M. Terahertz spectroscopy and imaging—Modern techniques and applications. *Laser Photon. Rev.* **2011**, *5*, 124–166. [CrossRef]
17. Buchner, R.; Barthel, J.; Stauber, J. The dielectric relaxation of water between 0 °C and 35 °C. *Chem. Phys. Lett.* **1999**, *306*, 57–63. [CrossRef]

18. Bertie, J. E.; Lan, Z. Infrared intensities of liquids XX: The intensity of the OH stretching band of liquid water revisited, and the best current values of the optical constants of. *Appl. Spectrosc.* **1996**, *50*, 1047–1057. [CrossRef]
19. Zhou, J.; Rao, X.; Liu, X.; Li, T.; Zhou, L.; Zheng, Y.; Zhu, Z. Temperature dependent optical and dielectric properties of liquid water studied by terahertz time-domain spectroscopy. *AIP Adv.* **2019**, *9*, 035328. [CrossRef]
20. Tonouchi, M. Cutting-edge terahertz technology. *Nat. Photon.* **2007**, *1*, 97–105. [CrossRef]
21. Baxter, J.B.; Guglietta, G.W. Terahertz spectroscopy. *Anal. Chem.* **2011**, *83*, 4342–4368. [CrossRef]
22. Cytiva Life Sciences. Amersham Protran 0.2 NC Nitrocellulose Membranes. 2025. Available online: https://www.cytivalifesciences.com/en/fi/shop/protein-analysis/blotting-and-detection/blotting-membranes/amersham-protran-0-2-nc-nitrocellulose-western-blotting-membranes-p-00169 (accessed on 18 May 2025).
23. Davies, C.L.; Patel, J.B.; Xia, C.Q.; Herz, L.M.; Johnston, M.B. Temperature-dependent refractive index of quartz at terahertz frequencies. *J. Infrared Millimeter Terahertz Waves* **2018**, *39*, 1236–1248. [CrossRef]
24. Li, A.; Wang, Y.; Deng, L.; Zhao, X.; Yan, Q.; Cai, Y.; Lin, J.; Bai, Y.; Liu, S.; Zhang, Y. Use of nitrocellulose membranes as a scaffold in cell culture. *Cytotechnology* **2013**, *65*, 71–81. [CrossRef]
25. Fridley, G.E.; Holstein, C.A.; Oza, S.B.; Yager, P. The evolution of nitrocellulose as a material for bioassays. *MRS Bull.* **2013**, *38*, 326–330. [CrossRef]
26. Katsidis, C.C.; Siapkas, D.I. General transfer-matrix method for optical multilayer systems with coherent, partially coherent, and incoherent interference. *Appl. Opt.* **2002**, *41*, 3978–3987. [CrossRef] [PubMed]
27. Fiedler, J.; Boström, M.; Persson, C.; Brevik, I.; Corkery, R.; Buhmann, S.Y.; Parsons, D.F. Full-spectrum high-resolution modeling of the dielectric function of water. *J. Phys. Chem. B* **2020**, *124*, 3103–3113. [CrossRef] [PubMed]

Disclaimer/Publisher's Note: The statements, opinions and data contained in all publications are solely those of the individual author(s) and contributor(s) and not of MDPI and/or the editor(s). MDPI and/or the editor(s) disclaim responsibility for any injury to people or property resulting from any ideas, methods, instructions or products referred to in the content.